

Lunar Gravity, Topography and Crustal Thickness Archive

This archive contains lunar gravity, topography, and crustal thickness data and images that were presented in *Wieczorek et al.* (2006). The crustal thickness models use the Clementine topography of *Smith et al.* (1997; GLTM2C) and the Lunar Prospector LP150Q gravity model of *Konopliv et al.* (2001). The thickness of the mare basalts within the large basins is based on the model of *Solomon and Head* (1980), modified by the maximum basalt thicknesses of *Williams and Zuber* (1999). Additional modifications from previous crustal thickness models (*Wieczorek and Phillips*, 1998, 1999) include the following:

1. The bouguer correction was not filtered as the power spectrum of the LP150Q gravity model is realistic up to degree 65.
2. The gravity and topography fields were used only up to degree 65.
3. When inverting for the relief along the crust-mantle interface, the downward continuation filter of *Wieczorek and Phillips* (1998) was chosen such that this filter had a value of 0.5 at degree 30.
4. The crustal thickness at the Apollo 12/14 site was anchored by the seismic velocity model of *Khan et al.* (2000); the total crustal thickness was assumed to be 45 km, and the intracrustal seismic discontinuity (for the dual-layered model) was assumed to be located 20 km beneath the surface.

Model 1

This is the "traditional" single layer crustal thickness model in which the gravitational field is assumed to be a result of surface and Moho relief, and mare basalt fill. This model has a minimum crustal thickness (excluding the mare fill) of almost zero km beneath the Crisium basin, and a maximum thickness of about 154 km.

Model 2

The only difference between this model and Model 1 is that the degree-1 gravitational attraction of the surface topography (i.e., the Bouguer correction) was set to zero before inverting for the relief along the crust-mantle interface. This model implicitly assumes that the degree-1 Bouguer correction is compensated by degree-1 heterogeneities in either mantle or crustal density (that is, either the near side mantle or crust is denser than the farside mantle or crust, respectively). This model has a minimum crustal thickness of about zero beneath the Apollo basin, and a maximum thickness of about 104 km.

Model 3

This is a dual-layered crustal thickness model in which the upper crust is allowed to vary in thickness, but the lower crust is constrained to have a constant thickness of 25 km. Wherever the gravity field could not be satisfied by these assumptions (such as beneath the large impact basins), the thickness of the lower crust was allowed to vary as well. Note that this model is different than the preferred dual-layered model of *Wieczorek and Phillips* (1998). This model has a minimum crustal thickness (excluding mare fill) of almost zero km beneath the Crisium basin, and a maximum crustal thickness of about 134 km.

Model Parameters

Parameter	Model 1	Model 2	Model 3
Reference crustal thickness (km)	53.4	43.4	52.0
Density of upper crust (kg/m ³)	2900	2900	2820
Density of lower crust (kg/m ³)	NA	NA	3040
Density of mantle (kg/m ³)	3320	3400	3350
Density of mare basalts (kg/m ³)	3300	3300	3300

Archive Contents

Model 1: Single Layer Crust

moho_single_1.sh	Spherical harmonic coefficients for the radius of the crust-mantle interface.
single_1_thick_total.dat	Total crustal thickness.
single_1_thick_wo_mare.dat	Total crustal thickness, excluding contribution of mare fill.
single_1_thick_total_mol.pdf	Total crustal thickness image in a Mollweide projection (center meridian at 90W).
single_1_thick_total.pdf	Total crustal thickness image in two hemispheric Lambert azimuthal equal area projections.
basins_single_1.pdf	Crustal thickness images of the major nearside impact basins. All images are in Albers equal-area projections. Note that the crustal thickness determinations for the farside portions of Smythii, Humboldtianum, Orientale and Mendel-Rydberg may be inaccurate because of the lack of farside gravity coverage.

Model 2: Single Layer Crust, Degree-1 Bouguer Correction Set To Zero

moho_single_2.sh	Spherical harmonic coefficients for the radius of the crust-mantle interface.
single_2_thick_total.dat	Total crustal thickness.
single_2_thick_wo_mare.dat	Total crustal thickness, excluding contribution of mare fill.
single_2_thick_total_mol.pdf	Total crustal thickness image in a Mollweide projection (center meridian at 90W).
single_2_thick_total.pdf	Total crustal thickness image in two hemispheric Lambert azimuthal equal area projections.
basins_single_2.pdf	Crustal thickness images of the major nearside basins. All images are in Albers equal-area projections. Note that the crustal thickness determinations for the farside portions of Smythii, Humboldtianum, Orientale and Mendel-Rydberg may be inaccurate because of the lack of farside gravity coverage.

Model 3: Dual-Layered Model

dual_intra.sh	Spherical harmonic coefficients for the radius of the intracrustal interface.
dual_moho.sh	Spherical harmonic coefficients for the radius of the crust-mantle interface.
dual_thick_total.dat	Total crustal thickness.
dual_thick_total_wo_mare.dat	Total crustal thickness, excluding mare fill.
dual_upper_thick_wo_mare.dat	Upper crustal thickness, excluding mare fill.
dual_thick_mol.pdf	Images of the upper crustal thickness (excluding mare fill) and total crustal thickness in a Mollweide projection (center meridian at 90W).
dual_thick.pdf	Images of the upper crustal thickness (excluding mare fill) and total crustal thickness in hemispheric Lambert azimuthal equal area projections.
basins_dual.pdf	Crustal thickness images of the major nearside basins. All images are in Albers equal-area projections. Note that the crustal thickness determinations for the farside portions of Smythii, Humboldtianum, Orientale and Mendel-Rydberg may be inaccurate because of the lack of farside gravity coverage.

Gravity

LP150Q.sh	Spherical harmonic coefficients of the lunar potential field LP150Q (<i>Konopliv et al.</i> , 2001)
LP150Q_geoid_90_j2.dat	First-order geoid of the Moon (LP150Q) truncated at degree 90 and with the J2 term removed, and ignoring the current tidal potential of the Earth.

LP150Q_grav_90_j2.dat	Radial gravity of the Moon (LP150Q) truncated at degree 90 and with the J2 term removed.
LP150Q_grav_150_j2.dat	Radial gravity of the Moon (LP150Q) expanded to degree 150 and with the J2 term removed.
LP150Q_geoid_90_j2_mol.pdf	Geoid of the Moon (LP150Q) truncated at degree 90 and with the J2 term removed. Mollweide projection with central meridian at 90W.
LP150Q_geoid_90_j2.pdf	Geoid of the Moon (LP150Q) truncated at degree 90 and with the J2 term removed. Two hemispheric Lambert azimuthal equal area projections.
LP150Q_grav_90_j2_mol.pdf	Geoid of the Moon (LP150Q) truncated at degree 90 and with the J2 term removed. Mollweide projection with central meridian at 90W.
LP150Q_grav_90_j2.pdf	Radial gravity field of the Moon (LP150Q) truncated at degree 90 and with the J2 term removed, determined at a radius of 1738 km. Two hemispheric Lambert azimuthal equal area projections.
LP150Q_grav_150_j2_mol.pdf	Radial gravity field of the Moon (LP150Q) expanded to degree 150 and with the J2 term removed, determined at a radius of 1738 km. Mollweide projection with central meridian at 90W.
LP150Q_grav_150_j2.pdf	Radial gravity field of the Moon (LP150Q) expanded to degree 150 and with the J2 term removed, determined at a radius of 1738 km. Two hemispheric Lambert azimuthal equal area projections.

Topography

gltm2c.sh	Clementine shape model (GLTM2C).
gltm2c_wo_mare.sh	Clementine shape model with the thickness of the mare basalts removed.
moon_srm.tif	Cylindrical lunar shaded relief map of <i>Rosiek and Aeschliman</i> (2001) (0.25x0.25 degree resolution).
gltm2c_LP150Q_90.dat	Topography of the Moon (GLTM2C) referenced to the entire geoid (LP150Q) truncated at degree 90.
gltm2c_LP150Q_90_mol.pdf	Topography of the Moon (GLTM2C) referenced to the full geoid (LP150Q), both truncated at degree 90. Mollweide projection with central meridian at 90W.
gltm2c_LP150Q_90.pdf	Topography of the Moon (GLTM2C) referenced to the full geoid (LP150Q), both truncated at degree 90. Two hemispheric Lambert azimuthal equal area projections.
Topo_shots_mol.pdf	All accepted Clementine elevation measurements, measured with respect to a spheroid of radius 1738 at the equator and with a flattening of 1/3234.93, which corresponds to the J2 portion of the geoid. Mollweide projection with central meridian at 90W.
Topo_shots.pdf	All accepted Clementine elevation measurements, measured with respect to a spheroid of radius 1738 at the equator and with a flattening of 1/3234.93, which corresponds to the J2 portion of the geoid. Two hemispheric Lambert azimuthal equal area projections.
mare_thick.dat	Mare thickness model.
Mare_mol.pdf	Mare thickness model. Mollweide projection with central meridian at 90W.
Mare.pdf	Mare thickness model. Two hemispheric Lambert azimuthal equal area projections.

File formats

All .dat files are in an ascii raster format where the first and last data values represent the latitude and longitude coordinates (90, 0) and (-90,360), respectively. The interval between data values is one degree, corresponding to a matrix having 181 latitudinal and 361 longitudinal elements. All values are in SI units, unless otherwise noted. All .sh files contain spherical harmonic coefficients with each line containing the degree, order, and cosine and

sine coefficients (i.e., l , m , Clm , Slm). Spherical harmonic models are referenced to a surface radius of 1738 km.

References

Konopliv, A.S., S.W. Asmar, and D.N. Yuan, Recent gravity models as a result of the Lunar Prospector mission, *Icarus*, 150, 1-18, 2001.

Khan, A., K. Mosegaard, and K.L. Rasmussen, A new seismic velocity model for the Moon from a monte carlo inversion of the Apollo lunar seismic data, *Geophys. Res. Lett.*, 27, 1591-1594, 2000.

Rosiek, M.R., and R. Aeschliman, Lunar shaded relief map updated with Clementine data (abstract), *Lunar Planet. Sci. XXXII (CD-ROM)*, 1943, 2001.

Solomon, S.C., and J.W. Head, Lunar mascon basins: Lava filling, tectonics, and evolution of the lithosphere, *Rev. Geophys. Space Phys.*, 18, 107-141, 1980.

Smith, D.E., M.T. Zuber, G.A. Neumann, and F.G. Lemoine, Topography of the Moon from Clementine lidar, *J. Geophys. Res.*, 102, 1591-1611, 1997.

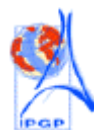
Wieczorek, M.A., and R.J. Phillips, Potential anomalies on a sphere: Applications to the thickness of the lunar crust, *J. Geophys. Res.*, 103, 1715-1724, 1998.

Wieczorek, M.A., and R.J. Phillips, Lunar multiring basins and the cratering process, *Icarus*, 139, 246-259, 1999.

Wieczorek, M. A. and 15 coauthors, The constitution and structure of the lunar interior, *Rev. Mineral. Geochem.*, 60, 221-364, 2006.

Williams, K.K., and M.T. Zuber, Measurements and analysis of lunar basin deposits from Clementine altimetry, *Icarus*, 131, 107-122, 1998.

Centre National de la Recherche
Scientifique
Institut de Physique du Globe de Paris
Equipe de Géophysique Spatiale et
Planétologie



Contact: [Mark Wieczorek](#)
Copyright © 2007 Mark
Wieczorek.
All Rights Reserved.